Determining Surface Roughness and Shape of Specular Diffuse Lobe Objects
Using Photometric Sampling Device[*]

Tesuo Kiuchi   Katsushi Ikeuchi

School of Computer Science
Carnegie Mellon University
Pittsburgh, PA 15213

ABSTRACT

The photometric sampling method extracts shape and reflectance properties of surfaces by using multiple illumination directions and a single viewing direction. We have previously proposed a recovering algorithm for smooth surfaces. One of the limitations of the previous algorithm is that it cannot recover the shape and roughness of specular lobe dominant surfaces. Surface reflection consists of three components: specular spike, specular lobe, and Lambertian. Among these three components, the previous method only can handle surfaces of the specular spike and the Lambertian.

This paper proposes a novel algorithm to recover surface shape and roughness of specular lobe dominant surfaces. An extraction algorithm uses the set of image brightness values measured at each surface point. Each brightness value provides one non-linear image irradiant equation, containing unknown parameters for surface orientation, reflectance and surface roughness. The algorithm iteratively solves the set of image irradiant non-linear equations with respect to these parameters. The experiments conducted on several rough surfaces show high accuracy in estimated orientations, and good estimation in surface roughness. We have demonstrated the ability of our method to detect surface defects on the rough gold surface of LSI package.

INTRODUCTION

Surface shape and roughness are important inspection criteria in industrial applications. For example, surface defects on a silicon wafer can be detected as points with non-mirror like reflection properties. A solder joint can be inspected from its appearance without electronic or mechanical methods. It can be judged good if its surface looks smooth and wet, and if its shape has gentle slopes. In many cases, the surface inspection of industrial products can be performed by comparing actual values and design values of shape and surface roughness. Therefore, we have developed an algorithm called the photosampler which can determine the shape and reflectance of a limited class of objects [2]. A set of images of the object are taken sequentially activating light sources whose locations and distributions are known. From this image sequence, surface reflectance and orientation can be calculated using a reflectance model.

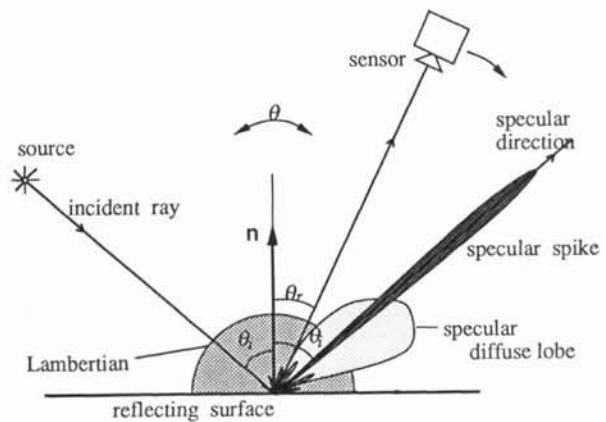Sato, Nayar and Ikeuchi [4] have built a 3D photosampling

Figure 1: Three component reflection model.

device and developed an algorithm to determine surface orientation based on a two component model: the Lambertian diffuse component and the specular spike component. The algorithm can be applied to smooth surfaces such as silicon wafers or transparent plastic lenses. However, since the algorithm ignored the specular diffuse lobe component, it can not be applied to rough surfaces such as solder joints or sand-blast finished surfaces.

This paper describes a method to determine surface orientation and roughness of specular diffuse lobe dominant surfaces.

SPECULAR DIFFUSE REFLECTION MODEL

Our surface reflection model consists of three components: Lambertian diffuse, specular spike and specular diffuse lobe [3]. See Figure 1. For a very smooth surface, the spike component dominates, and the surface looks like a mirror. As a surface becomes rougher, the mirror-like spike component shrinks rapidly, and the specular diffuse lobe component begins to dominate. Typical specular diffuse lobe dominant surfaces include: a "cold" solder joint which has been melted and resolidified, or metal finished by sand-blasting. The Lambertian diffuse component is considered to be body reflection which originates from inside a dielectric material like a plastic or a ceramic. The three component model is useful for describing material type and surface finish.

The specular diffuse lobe component is also a function of surface roughness. Surface roughness is a statistical func-

tion. The appearance of a specular diffuse lobe dominant surface can vary from shiny to blurred. Our model for the specular diffuse lobe component is based on the Beckmann-Spizzichino physical optics model [1] and the Torrance-Sparrow geometrical optics model [5].

$$L_{rad} = cG \frac{L_{irr} d\omega_i}{\cos \theta_r} \exp - \frac{\alpha^2}{2\sigma_\alpha^2}, \qquad (1)$$

where G and σ_α represent the geometric attenuation factor and the surface roughness parameter, respectively. The angle, α is measured as the difference betweeen the surface orientation and the bisector of the viewing and the light source direction. This model corresponds to the second term of the Beckmann-Spizzichino model; the specular diffuse lobe component. Although, the model is very simple, we have confirmed that it provides a good approximation of the specular diffuse lobe component of the Beckmann-Spizzichino model. See [5] for more details.

PHOTOSAMPLER APPARATUS

Figure 2 shows a photograph of the experimental device. The photosampler has lamps and a sphere made of light-diffusing material. The spherical diffuser is illuminated by an outside lamp, and generates an extended light source toward its inside. The object is placed at the center of the spherical diffuser, and is viewed by a TV camera through a hole at the top of the diffuser.

The process of measuring image brightness for different source directions is equivalent to sampling the image irradiance equation, $I'(\vec{S})$, at various $\vec{S}_i$. We distribute an array of extended sources around the object such that each source illuminates the object from a different direction. The entire array of extended sources may be scanned by sequentially activating each source one at a time and taking an image. Therefore, the scanning process results in a set of brightness, $I_i : i = 1, \ldots, M$, measured at each point on the object surface. M equals the number of extended light sources.

Figure 2: the photosampler device

MEASUREMENT THEORY

In this section we offer a method to measure surfaces that have specular diffuse lobe reflection. This method can measure surface orientation, reflectance, and surface roughness by using the photosampler. In the following discussion, the origin of the viewer center coordinate system is defined as the sphere center, and the Z axis corresponds with the optical axis of the TV camera.

The image irradiance equation for a surface with a specular diffuse lobe is derived for the photosampler. θ_n and ϕ_n denote surface orientation. The radiance of incident light L_{irr} in the reflection model(1) is substituted with the distribution of an extended light source L_i, which is a function of θ, ϕ and the direction of the i-th light source; θ_{s_i}, ϕ_{s_i}. The reflection angle θ_r is always equal to θ_n in the photosampler. Thus, an image irradiance equation for the i-th light source is:

$$I_i = \int_0^{2\pi} \int_0^{\pi/2} cG \frac{L_i(\theta_{s_i}, \phi_{s_i}; \theta, \phi)}{\cos \theta_n}$$
$$\exp - \frac{\alpha(\theta_n, \phi_n; \theta, \phi)^2}{2\sigma_\alpha^2} \sin \theta d\theta d\phi \qquad (2)$$

M image irradiance equations are obtained from M light sources. The goal is to solve these integral equations and obtain the surface parameters; θ_n, ϕ_n and σ_α.

When $\theta_n > \pi/2$, the surface cannot be seen by the TV camera, and its irradiance must be 0. The irradiance is symmetrical to the plane $\phi_{s_i} = \phi_n$. However, because of $1/\cos\theta$ the irradiance takes a maximum value at a certain θ_n larger than $\theta_s/2$. A surface illuminated by a light source at a lower longitude looks brighter than a surface which is illuminated by a light source at a higher longitude. Because of the geometric attenuator factor, the irradiance of the surface shrinks rapidly when θ_n approaches $\pi/2$.

These integral equations cannot be solved analytically. Even by numerical computing, it requires a tremendous amount of calculation to compute these integrals iteratively for combinations of the multidimensional parameters. We intend to approximate these equations by functions which are simple and easy to handle.

We numerically computed the irradiance diagrams described by Equation(2), and found the approximate image irradiance equation.

$$I_i = B + \frac{A}{\cos \theta_n} \exp(-\frac{\beta(\theta_n, \phi_n; \theta_{s_i}, \phi_{s_i})^2}{\sigma_\beta^2}) \qquad (3)$$

where β denotes the angle between the specular and the normal directions. The definition of the angle β is different from the definition of the angle α. σ_β is a function of convolution of the extended light source and the specular diffuse lobe. Therefore, its value is always larger than that of σ_α. The parameter A represents the reflectance multiplied by the radiance of a light source. Mutual reflections occur on the inside surfaces of the spherical diffuser, and they produce a uniform illumination. The parameter B represents the uniform irradiance by the mutual illumination, and its value should be equal to an irradiance by a light source beneath the horizon of the observed surface.

The five parameters: $\theta_n, \phi_n, \sigma_\beta, A, and B$, should be determined from these M approximate image irradiance equations. These equations are still non-linear, and can not be solved directly. An error function comparing the actual image values, I'_i, and computed values, I_i, with the reflection model(3) is defined as:

$$f(\theta_n, \phi_n, \sigma_\beta, A, B; I'_1..I'_M) = \Sigma_{i=1}^M (I_i - I'_i)^2 \qquad (4)$$

A minimization problem of the non-linear function, f, needs to be solved. Because of β, partial derivative functions of this error function f can not be obtained analytically. For this reason, the simplex method was used.

176

EXPERIMENTAL RESULTS

This section describes experiments performed to evaluate the performance of our proposed method. By using the radius of the sphere, R, and the distance between a point light source and the sphere, H, we can express the radiance distribution function of an extended light source as

$$L(\vec{P}, \vec{S}; R, H) = \frac{C\,[(R+H)(\vec{S} \cdot \vec{P}) - R]}{[(R + H - R\,(\vec{S} \cdot \vec{P}))^2 + (R(1 - (\vec{S} \cdot \vec{P})^2)]^{\frac{1}{2}}} \quad (5)$$

where $\vec{P}$ denotes a unit vector to a point on the diffuser surface and $\vec{S}$ denotes the point light source direction.

The diameter of diffuser R is 355.6mm (14-inch). The photosampler has thirty-six 60W frosty incandescent light bulbs, which generate the extended light sources. The bulbs are located at 36 of the 42 vertices of one-frequency icosa-hedron [1]. The camera hole opened in the diffuser is 25.4mm (1-inch) in diameter. The complete imaging system has a physical resolution of 0.5mm (0.002 inches) per pixel width.

At first, we measured the surface orientations and the re-flectance of a cylinder of known shape. Next, we measured surface roughness of a surface roughness scale. Then, we applied the method to the surface of a PGA LSI-package to demonstrate the feasibility of the method in practical applications.

Surface orientations and reflectance

Figure 3(a) shows a brass cylinder whose size is three eighth inch in diameter and one inch in height. Its surfaces are finished by a sand blast process, using 100 to 170 grain glass beads. The cylinder looks blurry and shows an example of typical specular diffuse reflection. The surface orientation distribution obtained is shown in Figure 3(b), where the brass cylinder is placed so its central axis is parallel with the vertical axis of the image.

$$x = kR_c \sin \theta', \theta' = \begin{cases} \theta & \phi_n \geq 0, \\ -\theta & \phi_n < 0. \end{cases} \quad (6)$$

where R_c and k denote the diameter of the cylinder and total magnification of the images. Figure 3(c) shows the relation of x and $\sin\theta'$. x should be linear with $\sin \theta'$. The accuracy of the extracted surface orientation of the cylinder can be evaluated by checking the linearity of this relation. The relation of both is linear, and the error is less than 1.6 degree in the range of $-60 \deg \leq \theta' \leq 60 \deg$. Therefore, the surface orientations of the cylinder are extracted accurately.

Figure 3(d) shows the extracted parameter A, the value of which is proportional to reflectance of the brass cylinder. The value of the parameter A is constant across the cylinder surface, independent of surface orientation. The figure depicting the parameter A looks bumpy compared to that of the surface orientation. This is because the surface roughness of the brass cylinder is not completely uniform and textures are observed in its images.

Surface roughness

We measured a surface roughness scale to ensure that surface roughness is also extracted correctly.

We used a Cast Microfinish Comparator C9 which is pro-duced by GAR, Danbury, CT . This surface roughness scale is
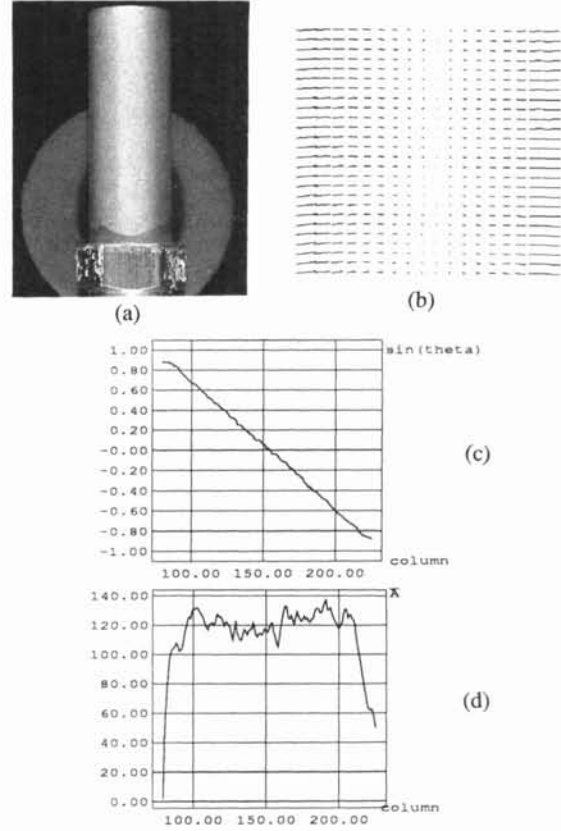

(a)　　　　(b)

(c)

(d)

Figure 3: Brass cylinder; (a) Brass cylinder, (b) Needle map, (c) Orientation plot, (d) Reflectance estimation.

a replica of cast surfaces finished through an electro forming process. It consists of specimens of 9 RMS roughness val-ues, ranging from 20 micro inches to 900 micro inches. The RMS roughness is defined under ANSI B46.1. The C9 scale is made by pure nickel, and will not corrode. See Figure 4(a) and (b).

The images of a specimen of 20 micro inches RMS rough-ness and 60 micro inches RMS roughness look similar and can hardly be distinguished by human eyes, while the images of specimens rougher than 120 micro inches show texture. We chose the 20 micro inches RMS roughness specimen and the 60 micro inches specimen, and compared the values of σ_β extracted by our measuring method.

Figure 4(c) shows this result. The values of parameter σ_β, which stands for surface roughness, is constant across the entire cylinder surface in both case of 20 micro inches specimen and 60 micro inches specimen. The values of the parameter σ_β extracted from 60 micro inches specimen are consistently larger than those from 20 micro inches specimen.

The values from the 60 micro inch specimen are less than three times of the values from the 20 micro inch specimen. It is because these σ_β values do not come from surface rough-ness alone. They are the result of the convolution of the extended light source and the specular diffuse lobe compo-nent of the surfaces illuminated by the extended light source.

Tables can be made which index the computed results of the convolution of the equation which depicts the extended light source and Gaussian functions which have σ_β values as RMS roughness. The real RMS roughness value can be obtained by searching these tables. Figure 4(c) indicates that
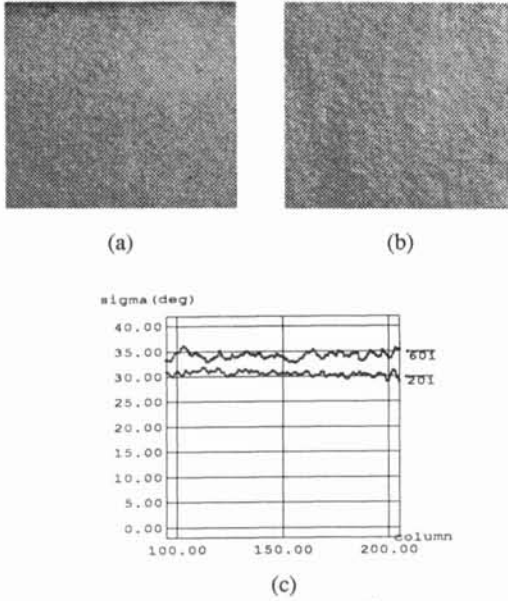
---

[1] A small section of the bottom hemisphere of the diffuser is not illumi-nated as light sources. This area is not observable from the TV camera.

(a)   (b)

(c)

Figure 4: Cast microfinish comparator; (a) Picture, 20 micro inches, (b) Picture, 60 micro inches, (c) Roughness estimation

(a)

(b)   (c)

Figure 5: PGA LSI package (a) Picture, (b) Distribution of A, (c) Distribution of σ_{β}.

surface roughness values are extracted.

PGA LSI package

Figure 5(a) shows a photograph of the base of a PGA LSI package on which a LSI chip is mounted and wire-bonded. A square bright area is heatsink made of gold. The gold area is a rough surface with texture. With careful observation, a defect on it looks like a stain. The performance of our method was tested by detecting this defect.

Figure 5(b) shows an image of the extracted parameter A. This is proportional to the reflectance of the gold area. The stained defective area is observed clearly.

Figure 5(c) shows an image of the extracted parameter σ_{β}. This represents the surface roughness of the same area. The defect is also observed clearly. These images indicate the reflectance and surface roughness change in the defective area.

The outside of the square portion of the LSI base is coated and protected by insulation. This insulation is transparent but dark. The reflectance of the coated gold decreased to a small amount, but the surface roughness did not change. Thus, the outside printed circuit is observed clearly in the image of σ_{β}, while the outside of the square looks dark in the image of A.

We conclude that the feasibility of our method for industrial application of visual inspection is shown.

CONCLUSION

We propose a method to determine surface orientation and roughness for specular lobe dominant surfaces. From the image sequence, surface reflectance and orientation are obtained by determining the parameters of the reflectance model. This paper verifies the validity of this approach by applying it to real specular lobe dominant surfaces and examining orientation errors.
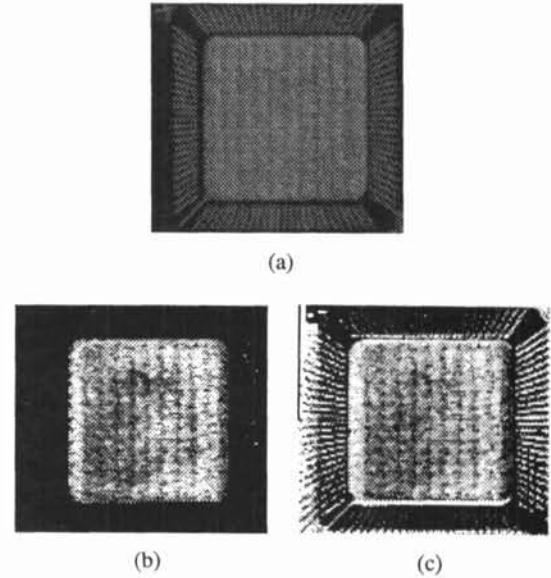
References

[1] P. Beckmann and A. Spizzichino. *The Scattering of Electromagnetic Waves from Rough Surfaces*. Pergamon Press, London, UK, 1963.

[2] S.K. Nayar, K. Ikeuchi, and T. Kanade. Determining shape and reflectance of hybrid surfaces by photometric sampling. *IEEE Trans. Robotics and Automation*, 6(4):418–431, August 1990.

[3] S.K. Nayar, K. Ikeuchi, and T. Kanade. Surface reflection: physical and geometrical perspectives. *IEEE Trans. Pattern Analysis and Machine Intelligence*, 13(7):661–634, July 1991.

[4] H. Sato, S. Nayar, and K. Ikeuchi. Extracting shape and reflectance of glossy surfaces by using 3D photometric sampling method. In *IAPR Workshop on Machine Vision Applications*, pages 82–88. IEEE Computer Society, November 1990.

[5] K.E. Torrance and E.M. Sparrow. Theory for off-specular reflection from roughened surfaces. *Journal of the Optical Socitey of America*, 57:1105–1114, September 1967.